12th Hel.A.S. Conference
Thessaloniki, 28 June - 2 July, 2015
CONTRIBUTED LECTURE

Modeling of plasma dynamics in the inner geospace during enhanced magnetospheric activity

C. Tsironis[1], *A. Anastasiadis*[1], *C. Katsavrias*[2,1] *and I. A. Daglis*[2]
[1]National Observatory of Athens, Greece
[2]National and Kapodistrian University of Athens, Greece

Abstract: We investigate the effect of substorms on the ring current buildup in the inner geospace, by means of numerical simulations of plasma ion dynamics during enhanced magnetospheric activity. A particle tracing model solves for the ion motion in a dynamic geomagnetic field, and the electric field due to convection, corotation and Faraday induction. The data from the test-particle simulations is used for analyzing the dependence on the initial conditions, as well as for a mapping of the different ion species to the storm-time magnetospheric currents. An estimation of the Dst index is given in terms of the ensemble-averaged ring and tail currents. The presented tool serves as the final link in a Sun-to-Earth modeling chain of major solar eruptions.

1 Introduction

During each solar cycle, sequences of coronal mass ejections arrive near Earth and trigger space weather effects like geomagnetic storms and magnetospheric substorms [1]. The associated dynamic processes evolve as energy loading-dissipation cycles in a variety of timescales, from days for storms to hours for substorms [2]. For numerous events, the system can be described by means of a few geomagnetic indices, like Kp and Dst, which can be derived from solar wind and IMF values. For the other cases, large-scale numerical solvers of the coupled solar wind-magnetosphere may be employed, which have advanced with the increased availability of computer resources. In this context, one may follow directly the 3D particle trajectories during the event phases under the effect of the electric and magnetic forces, which are the magnetic field superposition of the Earth's terrestrial magnet with the fields generated by the current sources, and the electric field owed to plasma convection, Earth-induced corotation and Faraday induction [3]. In this paper, we present results from the simulation of the dynamics of the energetic particles in the inner magnetosphere, focusing on the ring current buildup and decay when substorms are occurring, and on the estimation of the Dst index from the test-particle results.

2 Model description

The magnetic field in geospace is the sum of the Earth's terrestrial field and of the external field generated by the magnetopause current, the tail currents, the Birkeland currents and the ring current. The Earth's field $\mathbf{B_{ter}}$ is approximated as the one of a tilted dipole magnet placed at the geometrical center, with the poles directed in reverse with respect to the geographic ones, and varies slowly in comparison to the solar activity and its geomagnetic response. The external part $\mathbf{B_{ext}}$ is computed in terms of the Tsyganenko T89 model, which is driven by the geomagnetic parameter Kp [4]. For the visualization of $\mathbf{B}$, one employs the standard field-line tracing technique. In 2D, a clear picture (i.e. with minimal intersections between the field line projections) is provided only on the $(x, y = 0, z)$ plane, as a result from the geometric symmetries in the magnetosphere. In Figure 1a we show the magnetic field map for storm-time conditions ($Kp = 5$) in the typical tilt angle $\theta_t = 11.5$ deg. The dynamic part of the magnetic field is determined by the modification of the geomagnetic parameters in time. Introducing the vector $\mathbf{G} = [G_j] = [\theta_t, Kp]$, the magnetic field may be discretized and cast

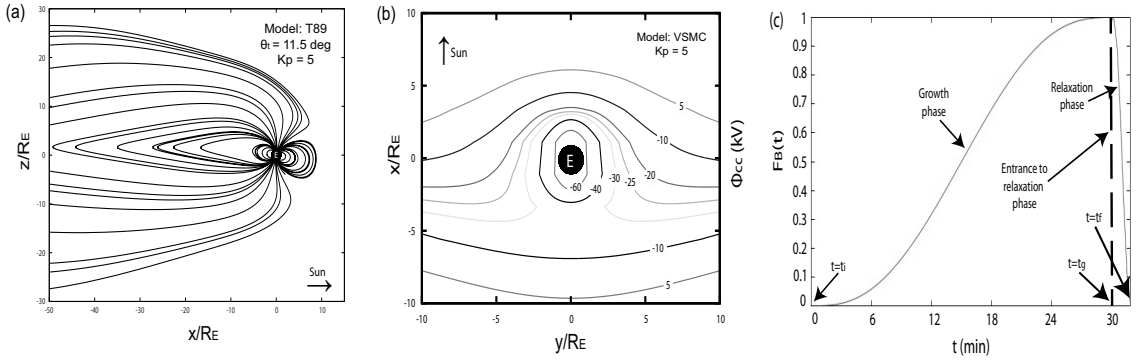

Figure 1: (a) Geomagnetic field map, as calculated with the T89 model, for $\theta_t = 11.5$ deg and $Kp = 5$, (b) Contour levels of the electrostatic potential, as calculated with the VSMC model, for $Kp = 5$, (c) Function F_B for the case of an isolated substorm with $t_i = 0$ min, $t_g = 30$ min and $t_f = t_r = 35$ min.

in the form $\mathbf{B}(\mathbf{r}, t) = \mathbf{B_{ter}}(\mathbf{r}) + \mathbf{B_{ext}}[\mathbf{r}, G_j(t_i)] + F_B(t) \cdot \{\mathbf{B_{ext}}[\mathbf{r}, G_j(t_f)] - \mathbf{B_{ext}}[\mathbf{r}, G_j(t_i)]\}$. In our model, an event starts at time t_i, stops at t_f and, during this interval, it evolves in phases described by the function F_B and the values of $\mathbf{G}$ at t_i and t_f. $F_B(t)$ is defined with the requirement that it simulates sufficiently the main properties of the studied event, as observed in measurements. Here, we refer to substorms, which have an initial growth period where the field strength is increasing to high values, followed by a relaxation phase where B returns to its previous level. In Figure 1c we illustrate $F_B(t)$ for a substorm event with timestamps $t_i = 0$ min, $t_g = 30$ min, $t_f = t_r = 35$ min. In its turn, the electric field is divided to three components: The one owed to plasma convection in the magnetosphere, the one due to near-Earth plasma corotation, and the one generated by the dynamic variation of $\mathbf{B_{ext}}$ during the event(s). The slow time-scale of the convection and corotation processes in comparison to the overall plasma dynamics allows for their consideration as static. For determining the electrostatic potential Φ_{cc} we employ the Volland-Stern-Maynard-Chen (VSMC) model, which is based on an empirical dawn-dusk potential distribution with Kp-dependence and magnetopause shielding [5]. Regarding visualization, the contour level surfaces are calculated by solving the model equation with respect to the coordinates. In Figure 1b we perform a 2D visualization of the contour lines on the equatorial plane ($z = 0$) for $Kp = 5$. The particle trajectory is traced by solving numerically Newton's second law of motion, $m\ddot{\mathbf{r}} = q(\mathbf{E} + d\dot{\mathbf{r}} \times \mathbf{B}) - mg_E R_E^2 r^{-3}\mathbf{r}$, where $g_E = 9.81$ m/s^2 is the gravitational acceleration on Earth's surface and m, q are the particle mass and electric charge. For electrons it is $m_e = 9.31 \cdot 10^{-31}$ kg and $q_e = -1.6 \cdot 10^{-19}$ Cb, while for an ion of atomic mass $\mathcal{A}_i$ and ionization rate s_i it is $m_i = 1837\mathcal{A}_i m_e$ and $q_i = s_i|q_e|$. The numerical code combines the models presented up so far (T89, VSMC, Newton-Lorentz), and the computation is interrupted in case the particle leaves the inner magnetosphere, either by precipitating on Earth ($r \leq R_E$), crossing the magnetopause or reaching a tailward distance further than $70R_E$, with different stop codes so that each case is distinguished.

3 Numerical results

The results from test-particle simulations in the occurrence of an isolated substorm are shown and analyzed. The particle starts its flight at $t = t_0$, which may be before ($t_0 - t_i < 0$) or after ($t_0 - t_i > 0$) the event onset, interacts with the substorm until t_r and continues moving in the restored fields until t_1. Three primary types of ion trajectories are found: (i) Orbits which become trapped inside the ring current, (ii) orbits that precipitate in Earth's atmosphere, and (iii) orbits escaping tailward or by crossing the magnetopause. In Figure 2a, we show the planar projection of the orbit of an O^+ ion that eventually integrates to the ring current. The motion starts at $t_0 = -8$ min with initial radius $r(t_0) = 20R_E$, magnetic local time (MLT) $\phi(t_0) = 24$ h, latitude $\theta(t_0) = 25$ deg, pitch angle $\alpha(t_0) = \pi/2$ and kinetic energy $E_k(t_0) = 4$ KeV, and is followed up to 2.5 hours after the event. In its course to the ring current, the ion is considerably accelerated from the energy exchange with the fields. 3D orbits corresponding to the other types of motion are also shown: The precipitating orbit is of an H^+ ion with $E_k(t_0) = 0.5$ KeV, whereas the escaping orbit is of an O^+ ion with $E_k(t_0) = 7$ KeV. In the former case,

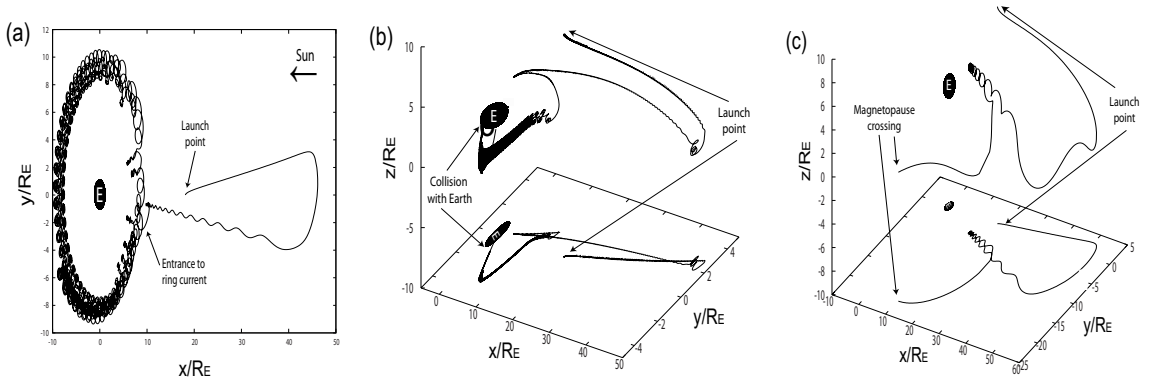

Figure 2: (a) Projection of a trapped O^+ orbit with $r(t_0) = 20R_E$, $\phi(t_0) = 24$ h, $\theta(t_0) = 25$ deg, $\alpha(t_0) = \pi/2$ and $E_k(t_0) = 4$ KeV, (b) 3D orbit of a precipitating H^+ for the same case apart from $E_k(t_0) = 0.5$ KeV, (c) 3D orbit of an escaping O^+ for the same case apart from $E_k(t_0) = 7$ KeV.

the H^+ particle sets off with a low initial energy and consequently ends up on the terrestrial atmosphere well before t_1, however the final energy is as large as in the previous case. The escaping O^+ ion starts with a relatively high value of energy and escapes the inner magnetosphere along the meridian before t_1 with a velocity gain. For the statistical analysis of the motions, in Figure 3 we present results for the final kinetic energy from different simulations where the initial conditions varied are $r(t_0)$ and $E_k(t_0)$. In the first computation, $r(t_0)$ took values in a loop from $2R_E$ to $30R_E$, whereas in the other case $E_k(t_0)$ ranged from 0.5 KeV to 20 keV, with all the rest of the quantities equal to the values already defined. The general picture is that the dependence of the particle dynamics on the initial conditions is very sensitive, which is imprinted in the wide regions where $E_k(t_1)$ exhibits an irregular variation over the values at $t = t_0$. However, in all cases one identifies consecutive regions where the ions either get accelerated or remain at low energy. In Figure 3a, there is a spatial region from $14R_E$ to almost $17R_E$ where all injected ions gain significant amounts of energy, as well as one within $21R_E$ and $25R_E$ where nearly all particles do not appear a net energization. In Figure 3b the probability of acceleration appears to be larger for O^+ ions with low energy at the event start ($Ek(t_0) < 6$ keV) than for initially energetic ions (having e.g. $Ek(t_0) > 15$ keV). The connection of Dst to the ring current and the contribution of each current source during the event phases are under debate. In many cases, Dst is assumed to be correlated with the ring current energy from storm maximum well into recovery, but, in some cases, it is also suggested that, during disturbances, Dst may also be related to other sources. For studies related to the inner magnetosphere, the connection of Dst with the energy of the ring current has been described in terms of the Dessler-Parker-Sckopke (DPS) relation, which connects the energy E_{pp} stored in a specific plasma population with the associated magnetic perturbation [6]. Introducing a correction term for the magnetopause current in the original relation, one obtains the modified equation $Dst = -\mu_0(2\pi B_E R_E^3)^{-1} \sum_{pp} E_{pp} + b_{dps}\sqrt{P_{dyn}} + c_{dps}$, where b_{dps} is associated to the magnetopause correction and c_{dps} to the quiet-time energy level. In the simulations, the ring current particles are assumed to be confined inside a torus with radii $R_{rc} = 6R_E$ and $r_{rc} = 3R_E$ (i.e. extending from $3R_E$ to $9R_E$), whereas the near-Earth tail region is defined as the remaining area in the simulation box ranging within $[r_{rc}, r_{rc} + R_{ntl}]$ along the Sun-Earth axis and $[-R_{ntl}, R_{ntl}]$ in the other two directions, with $R_{ntl} = 20R_E$. The energies E_{rc}, E_{ntl} of the ring and near-tail current particles are described over the average energy of H^+ and O^+ test ions that belong to these currents, which are computed, at each time step, over the particles contained inside the specific region at that time. The result of the Dst computation using the scheme described above are presented in Figure 3. The event scenario explored is again the one introduced above, in which 1000 oxygen ions were launched from the plasma sheet and 1000 hydrogen ions were started in the ring current. The initial conditions for the MLT and the pitch angle were the same for both species, whereas the initial radii, latitudes and kinetic energies were assigned randomly within different ranges. In computing the Dst index, it was assumed that $P_{dyn} = 4$ nPa, $b_{dps} = 7.26$ nT/nPa$^{1/2}$, $c_{dps} = -11$ nT, $n_{rc,O} = n_{rc,H} = 10$ cm^{-3} and $n_{ntl,O} = n_{ntl,H} = 1$ cm^{-3}. In Figure 3c we plot the dynamic evolution of Dst, and the contributions from the ring current and the near-Earth tail plasma distributions to its value are given for comparisons.

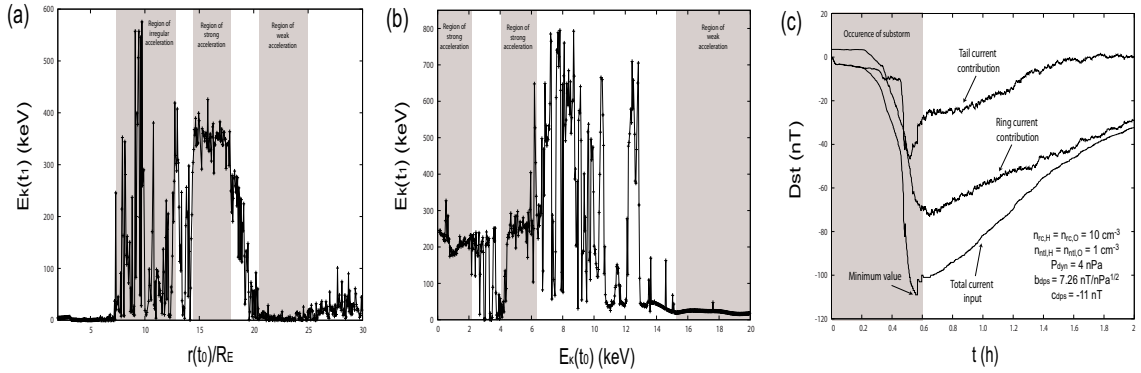

Figure 3: (a) $E_k(t_1)$ from 1000 O^+ particles with initial conditions, unless otherwise stated, same as in Figure 1, vs $r(t_0)$ for $2R_E < r(t_0) < 30R_E$, (b) The same vs $E_k(t_0)$ for 0.5 keV< $E_k(t_0)$ <20 keV, (c) Dynamic evolution of Dst and of its ring/tail current contributions, based on an ensemble of 2000 test ions, 1000 O^+ launched from the plasma sheet and 1000 H^+ in the ring current.

During the substorm growth, Dst decreases continuously, with the most rapid variation being around the interchange from growth to relaxation phase, and the smallest values of Dst persist for long times after the event termination. Overall, the effect of the ring current is larger than the one coming from the energetic particles in the near-Earth tail region. The contribution of the tail current is measurable up to $t = 1.2$ h, with a maximum near the end of the event growth ($t = 0.55$ h), and from there on the Dst is essentially determined only by the ring current. The contribution to Dst by the tail current is found equal to 30% on the average, close to the reported figure of 25%.

4 Conclusions

In this work, we have investigated the dynamic evolution of the near-Earth current populations during the occurrence of magnetospheric substorms. The analysis of test-particle orbits reveals fragments of the ion dynamics, among which three main types of substorm-driven ion orbits (trapped, precipitating and escaping). The addition of the induced electric field component to the convection provides a mechanism for the observed energization levels of ions which drift towards the ring current region. Further analysis of the ion motions reveals a sensitive dependence of the particle dynamics on the initial conditions. For the effect of each current source to the Dst index, we have concluded that the dependence of Dst also on other effective sources, apart from the ring current energy, should be considered.

Acknowledgements: This research has been co-financed by the European Union (European Social Fund) and Greek national funds through the Operational Program "Education and Lifelong Learning" of the National Strategic Reference Framework Research Funding Program: Thales. Investing in knowledge society through the European Social Fund.

References

[1] Patsourakos, S., et al: 2015, Astrophys. J., submitted.

[2] Daglis, I.A., et al: 1999, Rev. Geophys. 37, 407.

[3] Delcourt, D.C.: 2002, J.A.S.T.P. 64, 551.

[4] Tsyganenko, N.A.: 2013, Ann. Geophys. 31, 1745.

[5] Volland, H.: 1973, J. Geophys. Res. 78, 171.

[6] Kozyra, J.U., and Liemohn, M.W.: 2003, Space Sci. Rev. 109, 105.